

Stable discretisations of high-order discontinuous Galerkin methods on equidistant and scattered points

Jan Glaubitz^{a,b,*}, Philipp Öffner^c

^aMax Planck Institute for Mathematics, Bonn, Germany

^bInstitute for Computational Mathematics, TU Braunschweig, Braunschweig, Germany

^cInstitut für Mathematik, Universität Zürich, Zürich, Switzerland

Abstract

In this work, we propose and investigate stable high-order collocation-type discretisations of the discontinuous Galerkin method on equidistant and scattered collocation points. We do so by incorporating the concept of discrete least squares into the discontinuous Galerkin framework. Discrete least squares approximations allow us to construct stable and high-order accurate approximations on arbitrary collocation points, while discrete least squares quadrature rules allow us their stable and exact numerical integration. Both methods are computed efficiently by using bases of discrete orthogonal polynomials. Thus, the proposed discretisation generalises known classes of discretisations of the discontinuous Galerkin method, such as the discontinuous Galerkin collocation spectral element method. We are able to prove conservation and linear L^2 -stability of the proposed discretisations. Finally, numerical tests investigate their accuracy and demonstrate their extension to nonlinear conservation laws, systems, longtime simulations, and a variable coefficient problem in two space dimensions.

Keywords: hyperbolic conservation laws, high-order methods, discontinuous Galerkin methods, scattered nodes, discrete least squares, numerical integration, discrete orthogonal polynomials

1. Introduction

In the last decades, great efforts have been made to develop accurate and stable numerical methods for time-dependent partial differential equations (PDEs), especially for hyperbolic conservation laws

$$u_t + f(u)_x = 0. \quad (1)$$

The entropy solution of (1) satisfies the additional entropy condition

$$U(u)_t + F(u)_x \leq 0 \quad (2)$$

in the sense of distributions. U is a convex entropy function and F is a corresponding entropy flux satisfying $U'f' = F'$. A strict inequality in (2) reflects the existence of physically reasonable shock waves.

Traditionally, low-order numerical schemes, for instance classical finite volume (FV) methods, have been used to solve hyperbolic conservation laws, particularly in industrial applications. But since they become quite costly for high accuracy or long time simulations, there is a rising demand of high-order (third and above) methods. These have the potential of providing accurate solutions at reasonable costs. In this work, we consider the particularly popular class of discontinuous Galerkin (DG) finite element methods for hyperbolic conservation laws (1). These methods were first introduced 1973 by Reed and Hill [RH73] to

*Corresponding author

Email address: j.glaubitz@tu-bs.de (Jan Glaubitz)

solve the hyperbolic neutron transport equation in a nuclear reactor and were put on mathematically solid ground by Cockburn, Shu, and co-authors in a series of papers [CS91, CS89, CLS89, CHS90, CS98] around 1990. In [CS89] and [CHS90] it was proven that the resulting class of DG methods is (formally) high-order accurate in smooth regions, total-variation bounded in one space dimension, and maximum-norm bounded in any number of space dimensions. Further, Jiang and Shu proved in [JS94] a cell entropy inequality for the square entropy

$$U(u) = \frac{u^2}{2} \quad (3)$$

of linear as well as nonlinear scalar conservation laws for the DG method. It should be noted that this result does not need any nonlinear limiting as introduced in [CS89] and [CHS90]. The cell entropy inequality makes the DG method consistent with the entropy condition (2) and implies L^2 -stability of the scheme. Yet, Jiang and Shu's proof relies on exact evaluation of integrals and thus only applies to the *analytical* DG method, where all arising integrals are evaluated exactly. Unfortunately, exact evaluation of integrals is often computationally impractical or, depending on the nonlinearity of the flux function f , even impossible and is hence usually replaced by numerical quadrature rules. Then, exactness (at least up to machine precision) can be guaranteed by a sufficiently great number of integration points. This was, for instance, investigated by Kirby and Karniadakis in [KK03]. Another alternative are so-called DG collocation spectral element methods (DGSEMs) [HW07]. In these methods, the solution u as well as the flux f are approximated by interpolation polynomials in each element and the corresponding interpolation points are further matched with the integration points, which results in highly efficient operators [Kop09]. A typical problem of such discretisation of the DG method is their instability, especially for nonlinear conservation laws, due to the reduced accuracy of the integrals. There are several possible stabilisation methods in the literature, such as minmod-type limiting [CS89, CHS90], artificial viscosity methods [PP06, KWH11, RGÖS18, GNA⁺19, ÖGR19], modal filtering [Van91, HK08, GÖS18, RGÖS18], finite volume sub-cells [HCP12, DZLD14, SM14, MO16], and many more. Yet, in [Gas13, KG14, GWK16b] Gassner, Kopriva, and co-authors have been able to construct a DGSEM which is L^2 -stable for certain linear (variable coefficient) as well as nonlinear conservation laws by utilising skew-symmetric formulations of the conservation law (1) and Summation-by-Parts (SBP) operators, which were first used and investigated in finite difference (FD) methods [KS74, Str94, Ols95a, Ols95b, NC99]. It should be stressed that the theoretical stability (in the sense of a provable L^2 -norm inequality) as well as the numerical stability (in the sense of stable interpolation polynomials and quadrature rules) of the DGSEM heavily rely on the usage of Gauss–Lobatto points and quadrature weights, which include the boundary nodes and are more dense there, see [Gas13, KG14]. In [RÖS16] these results have been extended to Gauss–Legendre points and quadrature weights, which do not include the boundary nodes but are still more dense there. A more general approach, ensuring entropy stability by using decoupled SBP operators was recently proposed in [CDRFC19] by Chen and coauthors. Their approach is quite general and will be addressed in greater detail in §5.3.

In this work, we describe a first step towards L^2 -stable DGSEM on equidistant and even scattered collocation points. Yet, when using equidistant points for the (interpolation) polynomials approximating u and f in the DGSEM, we run into the Runge phenomenon [Run01]. Adapting an idea of Gelb et al. [GPR08] from spectral collocation methods, we tackle this problem by making a somewhat maverick generalisation. Instead of usual polynomial approximations by interpolation on $K + 1$ points, we build the polynomial approximations by the method of discrete least squares, where the data at a greater number of $N > K + 1$ points is used. The method thus utilises more information from the underlying function. By going over to a higher number of nodal values than technically needed, polynomial discrete least squares approximations are known to provide high accuracy while also successfully suppressing Runge oscillations, even on equidistant points. Care also has to be taken when performing numerical integration on equidistant or even scattered collocation points. To prove conservation as well as L^2 -stability, quadrature rules which exactly evaluate polynomials of degree $2K$ are needed. While interpolatory quadrature rules of arbitrary high order of exactness can be constructed even on equidistant (and scattered) points, they quickly become unstable, see [Huy09]. Thus, for an exact as well as stable evaluation of integrals, we propose to use so-called *least squares quadrature rules*. These have been introduced by Wilson in [Wil70b, Wil70a] and since then only revisited by Huybrechs in [Huy09]. To the best of our knowledge, in particular, least squares quadrature

rules have never been investigated in a PDE solver before. Utilising discrete least squares approximations and stable high-order quadrature rules, we are able to prove conservation and linear L^2 -stability of the resulting discretisation of the DG method on equidistant and scattered points.

The rest of this work is organised as follows. In §2, we revisit DG methods (without additional stabilisation) and their usual collocation-type discretisation on Gauss–Lobatto points. §3 introduces the concepts of discrete least squares approximations and least squares quadrature rules, which will provide stable and high-order numerical integration on equidistant and even scattered points. Their efficient computation is based on bases of discrete orthogonal polynomials. Building up on these concepts, we propose our stable high-order discretisation of the DG method on equidistant and scattered points in §4. The resulting discretisation of the DG method, which is based on the concept of discrete least squares, is referred to as the *DG discrete least squares (DGDLS) method* and generalises the usual discretisation of the DG method by the DGSEM. Conservation as well as linear L^2 -stability of the DGDLS method are proven in §5. In §6, numerical tests demonstrate conservation and L^2 -stability of the proposed DGDLS method for the linear advection equation and the nonlinear inviscid Burgers’ equation. Further, we investigate accuracy of the method and address the extension to systems of conservation laws, longtime simulations, and a variable coefficient problem in two spatial dimensions. We close this work with a summary and outlook in §7.

2. The discontinuous Galerkin method and its discretisation

Decoupling space and time by the method of lines [LeV02], DG methods are designed as semidiscretisations of hyperbolic conservation laws,

$$u_t + f(u)_x = 0, \quad (4)$$

on a computational domain Ω . In the following, we will only consider conservation laws in one dimension, i. e. $\Omega \subset \mathbb{R}$. For sake of simplicity, we further assume (4) to be a scalar conservation law for the moment. The extension of the later proposed discretisation will be addressed in §6.3. We refer to the function $u = u(t, x)$ as the *conservation variable* and to f as the *flux function*. The resulting system of ordinary differential equations (ODEs)

$$\frac{d}{dt}u = L(u), \quad (5)$$

where $L(u)$ is a discretisation of the spatial operator, can be solved by any time integration method. In this work, we use the explicit strong stability preserving (SSP) Runge–Kutta (RK) method¹ of third order using three stages (SSPRK(3,3)) given in [GS98] by Gottlieb and Shu: Let u^n be the solution at time t^n , then the solution u^{n+1} at time t^{n+1} is obtained by

$$\begin{aligned} u^{(1)} &= u^n + \Delta t L(u^n), \\ u^{(2)} &= \frac{3}{4}u^n + \frac{1}{4}u^{(1)} + \frac{1}{4}\Delta t L(u^{(1)}), \\ u^{n+1} &= \frac{1}{3}u^n + \frac{2}{3}u^{(2)} + \frac{2}{3}\Delta t L(u^{(2)}). \end{aligned} \quad (6)$$

For this method, in particular, L^2 -stability will also hold in time if it is ensured for the simple explicit Euler method. For more details about (TVD/SSP) RK methods see the extensive literature [GS98, LT98, GST01, Ket08, GKS11]. The later numerical tests in §6 have all been performed using the timestep size

$$\Delta t = \frac{C}{I(K+1)\lambda} \quad (7)$$

with $C = 0.1$ and where $\lambda = \max_u |f'(u)|$ is the fastest propagation speed. In the following, we discuss the discretisation $L(u)$ of the spatial operator given by the DG method.

¹SSP-RK methods are a generalisation of TVD-RK methods, where instead of the total variation of the solution u every convex functional of the solution u is ensured to decrease if this holds for a step of the simple explicit Euler method.

2.1. The analytical discontinuous Galerkin method

DG methods are obtained in the following way. First, the computational domain Ω is subdivided into smaller elements Ω_i for $i = 1, \dots, I$ with $\Omega = \bigcup_{i=1}^I \Omega_i$. In one dimension, the elements are given by simple subintervals

$$\Omega_i = \left(x_{i-\frac{1}{2}}, x_{i+\frac{1}{2}} \right), \quad (8)$$

which are typically mapped to a single reference element $\Omega_{\text{ref}} = (-1, 1)$ where all computations are performed. In two or more space dimensions, the elements might be given by triangles, tetrahedrons or other simple geometric objects. The conservation law (4) is solved in a weak form for every element then. On an element Ω_i , equation (4) is multiplied by a test function v and integrated in space. Integration by parts yields the weak form

$$\int_{\Omega_i} u_t v \, dx - \int_{\Omega_i} f(u) v_x \, dx + f\left(u(x_{i+\frac{1}{2}})\right) v(x_{i+\frac{1}{2}}) - f\left(u(x_{i-\frac{1}{2}})\right) v(x_{i-\frac{1}{2}}) = 0. \quad (9)$$

Now assume that both the solution u as well as the test function v come from a finite dimensional approximation space V_h , which is usually chosen to be the space of piecewise polynomials of degree at most K , i. e.

$$V_h = \left\{ v : \Omega \rightarrow \mathbb{R} \mid v^i := v|_{\Omega_i} \in \mathbb{P}_K(\Omega_i) \right\}. \quad (10)$$

It should be stressed that for this choice $u, v \in V_h$ might be discontinuous at element interfaces. Thus, the boundary terms $f\left(u(x_{i\pm\frac{1}{2}})\right)$ and $v(x_{i\pm\frac{1}{2}})$ are not well defined. We distinguish between values from inside Ω_i , e. g.

$$u_{i-\frac{1}{2}}^+ = u^i(x_{i-\frac{1}{2}}), \quad u_{i+\frac{1}{2}}^- = u^i(x_{i+\frac{1}{2}}), \quad v_{i-\frac{1}{2}}^+ = v^i(x_{i-\frac{1}{2}}), \quad v_{i+\frac{1}{2}}^- = v^i(x_{i+\frac{1}{2}}) \quad (11)$$

and values from neighbouring elements $\Omega_{i-i}, \Omega_{i+i}$, e. g.

$$u_{i-\frac{1}{2}}^- = u^{i-1}(x_{i-\frac{1}{2}}), \quad u_{i+\frac{1}{2}}^+ = u^{i+1}(x_{i+\frac{1}{2}}), \quad v_{i-\frac{1}{2}}^- = v^{i-1}(x_{i-\frac{1}{2}}), \quad v_{i+\frac{1}{2}}^+ = v^{i+1}(x_{i+\frac{1}{2}}). \quad (12)$$

From conservation and stability (upwinding) considerations, we take a single valued *numerical flux*

$$f_{i+\frac{1}{2}}^{\text{num}} = f^{\text{num}}\left(u_{i+\frac{1}{2}}^-, u_{i+\frac{1}{2}}^+\right) \quad (13)$$

to replace $f\left(u(x_{i+\frac{1}{2}})\right)$. Further, the numerical flux is consistent ($f^{\text{num}}(u, u) = f(u)$), Lipschitz continuous, and monotone (f^{num} is nondecreasing in the first argument and nonincreasing in the second argument). Examples of commonly used numerical fluxes can be found in [CS89] and [Tor13]. Hence, the DG method is: Find $u \in V_h$ such that

$$\int_{\Omega_i} u_t v \, dx - \int_{\Omega_i} f(u) v_x \, dx + f_{i+\frac{1}{2}}^{\text{num}} v_{i+\frac{1}{2}}^- - f_{i-\frac{1}{2}}^{\text{num}} v_{i-\frac{1}{2}}^+ = 0 \quad (14)$$

for all $v \in V_h$ and $i = 1, \dots, I$. Note that in (14) all integrals are assumed to be evaluated exactly. We thus refer to (14) as the *analytical DG method*. Finally, the analytical DG method (14) can be rewritten as a system of ODEs

$$\frac{d}{dt} u = L(u) \quad (15)$$

and the approximation $u \in V_h$ is evolved over time by some explicit TVD-RK method, as discussed before. Also see [CS89] and [HW07].

2.2. The discontinuous Galerkin collocation spectral element method

This subsection revisits the DGSEM in which u and f are both approximated by interpolation polynomials in each element and the corresponding interpolation points are matched with the integration points. We assume $u, v, f(u) \in V_h$, i.e. all functions are approximated by piecewise polynomials of degree up to K . Further, it is convenient to transform equation (4) for each element $\Omega_i = (x_{i-\frac{1}{2}}, x_{i+\frac{1}{2}})$ to the reference element $\Omega_{\text{ref}} = (-1, 1)$ via the linear map

$$x_i(\xi) = \bar{x}_i + \frac{\Delta x_i}{2} \xi, \quad (16)$$

where \bar{x}_i is the centre of the element Ω_i and Δx_i is its length. This results in the transformed equation

$$\frac{\Delta x_i}{2} u_t + f(u)_\xi = 0 \quad (17)$$

on $\Omega_{\text{ref}} = (-1, 1)$. By defining a set of $K + 1$ interpolation points $-1 \leq \xi_0 < \xi_1 < \dots < \xi_K \leq 1$ in the reference element, $u^i = u|_{\Omega_i}$ and $f^i = f(u)|_{\Omega_i}$ are computed by polynomial interpolation as

$$u^i(t, \xi) = \sum_{k=0}^K u_k^i(t) \ell_k(\xi) \quad \text{and} \quad f^i = \sum_{k=0}^K f_k^i \ell_k(\xi) \quad (18)$$

with time depended nodal values $u_k^i(t) = u^i(t, \xi_k)$, $f_k^i = f(u_k^i)$ at the interpolation points and corresponding Lagrange basis functions ℓ_k , which are defined by

$$\ell_k(\xi) = \prod_{j=0, j \neq k}^K \frac{\xi - \xi_j}{\xi_k - \xi_j} \quad (19)$$

and satisfy the cardinal property $\ell_k(x_j) = \delta_{kj}$. For sake of simplicity, we will just focus on the Gauss–Lobatto points for the interpolation as well as quadrature points $\{\xi_j\}_{j=0}^K$ and denote the associated quadrature weights by $\{\omega_j\}_{j=0}^K$. Analytic integration is replaced by the resulting quadrature rule

$$\int_{-1}^1 g(\xi) \, d\xi \approx \sum_{j=0}^K \omega_j g(\xi_j) \quad (20)$$

then. Besides the Gauss–Lobatto points, the Gauss–Legendre points are another typical choice for the collocation approach. Inserting these approximations into the DG formulation (14) and choosing $v^i = \ell_k$, we get the *DGSEM*: Solve

$$\omega_k \frac{\Delta x_i}{2} \frac{d}{dt} u_k^i - \sum_{j=0}^K \omega_j f_j^i \ell_k'(\xi_j) + f_{i+\frac{1}{2}}^{\text{num}} \ell_k(1) - f_{i-\frac{1}{2}}^{\text{num}} \ell_k(-1) = 0 \quad (21)$$

for all $k = 0, \dots, K$ and $i = 1, \dots, I$. Note that (21) is directly solved for the nodal degrees of freedom $\{u_k^i\}_{k=0, i=1}^{K, I}$ of the solution $u \in V_h$.

3. Discrete least squares approximations and quadrature rules

In this section, we revisit the concept of discrete least squares (DLS), which is closely related to (continuous) weighted inner products. The later proposed discretisation of the DG method on equidistant and scattered points is based on piecewise polynomial approximations of u and f . In every element, these approximations are computed by DLS approximations, which generalise polynomial interpolation. Further, exact integrals (in the analytical DGM) and usual Gauss–Lobatto quadrature rules (in the DGSEM), respectively, is replaced by stable high-order least squares quadrature rules (LS-QRs). The efficient implementation of both methods relies on bases of discrete orthogonal polynomials (DOPs).

3.1. Bases of discrete orthogonal polynomials

Let $N \in \mathbb{N}$, $\{\xi_n\}_{n=0}^N$ be a set of $N + 1$ distinct points in $[-1, 1]$, and $\underline{\omega} = [\omega_0, \dots, \omega_N]^T \in \mathbb{R}^{N+1}$ be a vector of corresponding positive weights. Then, in analogy to usual (continuous) inner products,

$$\langle u, v \rangle_{\underline{\omega}} := \sum_{n=0}^N \omega_n u(\xi_n) v(\xi_n) \quad (22)$$

is called a *discrete inner product*. An accompanying discrete norm is induced by

$$\|u\|_{\underline{\omega}}^2 = \langle u, u \rangle_{\underline{\omega}} = \sum_{n=0}^N \omega_n u(\xi_n)^2. \quad (23)$$

Now considering a basis $\{\varphi_k\}_{k=0}^K$ of $\mathbb{P}_K([-1, 1])$ with $K \leq N$, we call the basis elements *DOPs* if

$$\langle \varphi_k, \varphi_l \rangle_{\underline{\omega}} = \delta_{kl} \quad (24)$$

holds for $k, l = 0, \dots, K$, i.e. if they are orthogonal w.r.t. to the discrete inner product (22). For more details, we refer to the book [Gau04] of Gautschi. It should be stressed that for (nonclassical) DOPs often no explicit formula is known.² Thus, we utilise numerical algorithms to construct bases of DOPs, such as the Stieltjes procedure [Gau04] and the Gram-Schmidt process [TBI97]. In this work, we construct bases of DOPs by the numerical stable modified Gram-Schmidt process [TBI97] applied to an initial basis of Legendre polynomials.

3.2. Discrete least square approximations

Originally, DLS approximations are born from the wish to fit a linear mathematical model to given observations. In contrast to polynomial interpolation [PTK11], DLS approximations can be stable and highly accurate on equidistant and even scattered points. In this work, we use DLS approximations to fit polynomials $f_{K,N}$ of degree at most K to a greater number of N observations given by nodal values at the collocation points.

Let f be a function on $[-1, 1]$ which we only know at a set of $N + 1$ distinct points $\{\xi_n\}_{n=0}^N$ in $[-1, 1]$. The problem is to find a polynomial $f_{K,N} \in \mathbb{P}_K$ such that $f_{K,N} - f$ is minimised. Note that when we have a basis $\{\varphi_k\}_{k=0}^K$ of $\mathbb{P}_K([-1, 1])$, the polynomial $f_{K,N}$ can be represented as

$$f_{K,N}(\xi) = \sum_{k=0}^K \hat{f}_{k,N} \varphi_k(\xi), \quad (25)$$

where the $\hat{f}_{k,N}$ are the modal coefficients. Since we only know f at a set of $N + 1$ distinct points $\{\xi_n\}_{n=0}^N$, it is convenient to compare $f_{K,N}$ and f only at the points $\{\xi_n\}_{n=0}^N$. Thus, let us denote the vector of the known nodal values of f by $\underline{f} = (f(\xi_0), \dots, f(\xi_N))^T$, the vector of the modal coefficients of $f_{K,N}$ by $\underline{\hat{f}} = (\hat{f}_{0,N}, \dots, \hat{f}_{K,N})^T$, and the matrix which contains the values of the basis functions φ_k at the collocation points by

$$\underline{A} = (\varphi_k(\xi_n))_{k,n=0}^{K,N}. \quad (26)$$

Then, the problem can be reformulated as follows: Find $\underline{\hat{f}} \in \mathbb{R}^{K+1}$ such that $\underline{r} := \underline{A}\underline{\hat{f}} - \underline{f}$ is minimised, where \underline{r} is called the *residual vector*. In fact, there are many possible ways of defining a best approximation.

²At least for classical DOPs on equidistant points some formulas can, for instance, be found in the book of Gautschi [Gau04, Chapter 1.5.2]. These examples include the discrete Chebyshev polynomials, the Krawtchouk polynomials, the Charlier polynomials, the Meixner polynomials, and the Hahn polynomials.

In this work, we minimise $f_{K,N} - f$ w. r. t. discrete inner products and thus choose $f_{K,N}$ as the *DLS approximation* of f characterised by

$$\|f_{K,N} - f\|_{\underline{\omega}} = \min_{v \in \mathbb{P}_K} \|v - f\|_{\underline{\omega}}. \quad (27)$$

Since the discrete norm $\|\cdot\|_{\underline{\omega}}$ is induced by the discrete inner product (22), relation (27) is equivalent to

$$\langle f_{K,N} - f, v \rangle_{\underline{\omega}} = 0 \quad \forall v \in \mathbb{P}_K \quad (28)$$

and, when $f_{K,N}$ is represented w. r. t. a basis $\{\varphi_k\}_{k=0}^K$ of \mathbb{P}_K , yields a system of linear equations

$$\sum_{k=0}^K \hat{f}_{k,N} \langle \varphi_k, \varphi_i \rangle_{\underline{\omega}} = \langle f, \varphi_i \rangle_{\underline{\omega}}, \quad i = 0, \dots, K, \quad (29)$$

which can, for instance, be solved by Gaussian elimination. Yet, highest efficiency is obtained by choosing a basis of DOPs as discussed in §3.1. Then, the sum in (29) reduces to a single entry and the coefficients are given by

$$\hat{f}_{k,N} = \langle f, \varphi_k \rangle_{\underline{\omega}} \quad (30)$$

for $k = 0, \dots, K$. When computed by using bases of DOPs, DLS approximations are sometimes referred to as *DOP-LS approximations*, see [GPR08].

3.3. Stable high-order quadrature rules on equidistant and scattered points

In numerical integration, one approximates the continuous integral of a function g by finite sums over weighted nodal values of g at a set of distinct points, i. e.

$$I[g] := \int_{-1}^1 g(\xi) \, d\xi \approx \sum_{n=0}^N \omega_n g(\xi_n) =: Q_N[g], \quad (31)$$

where the QR Q_N is uniquely defined by the quadrature points $\{\xi_n\}_{n=0}^N$ and the quadrature weights $\{\omega_n\}_{n=0}^N$. In many applications, such as the discretisation of exact integrals in DG discretisations, the quadrature points are chosen as Gauss–Lobatto points and the quadrature weights are obtained by an interpolatory approach, resulting in the well-known Gauss–Lobatto QR; see [KS06, Gau11]. The Gauss–Lobatto QR provides a stable and highly accurate approximation and, when available, is often recommended. In particular, when at least $N + 1$ quadrature points are used, they provide order of exactness $d = 2N - 1$, i. e. polynomials of degree up to $d = 2N - 1$ are treated exactly and

$$Q_N[g] = I[g] \quad (32)$$

holds for all $g \in \mathbb{P}_{2N-1}$. Choosing $d = 2K - 1$ allows us to mimic integration by parts on a discrete level for our numerical solution $u \in \mathbb{P}_K$, since

$$Q_N[uu'] = \int_{-1}^1 uu' \, d\xi = u^2 \Big|_{-1}^1 - \int_{-1}^1 u'u \, d\xi = u^2 \Big|_{-1}^1 - Q_N[u'u] \quad (33)$$

is satisfied then. In this work, we are in need of QRs on equidistant or even scattered points. In this case, a first choice are composite Newton–Cotes QRs, such as the trapezoidal QR. Unfortunately, such QRs only provide small orders of exactness and will not allow us to construct conservative and stable high-order DG discretisations on equidistant and scattered points. Another option are general interpolatory QRs, where the QR is obtained by exactly integrating the interpolation polynomial g_N corresponding to the data set $\{(\xi_n, g(\xi_n)) \mid n = 0, \dots, N\}$, i. e.

$$Q_N[g] = \int_{-1}^1 g_N(\xi) \, d\xi \quad (34)$$

with $g_N \in \mathbb{P}_N$ such that $g_N(\xi_n) = g(\xi_n)$ for $n = 0, \dots, N$. Interpolatory QRs naturally yield at least order of exactness N , since $g_N = g$ for $g \in \mathbb{P}_N$. Yet, interpolatory QRs are known to become unstable on equidistant points for $N \rightarrow \infty$, see [Huy09]. Let $\underline{\omega} = (\omega_0, \dots, \omega_N)^T$ be a vector of quadrature weights. A common measure of stability of a QR is given by

$$\kappa(\underline{\omega}) := \sum_{n=0}^N |\omega_n|. \quad (35)$$

We call a QR with weights $\underline{\omega}$ *stable*, if κ is uniformly bounded w. r. t. N , i.e.

$$\sup_{n \in \mathbb{N}} \kappa(\underline{\omega}) = C < \infty. \quad (36)$$

The idea behind this concept is that for a perturbed input \tilde{g} with $|g(\xi) - \tilde{g}(\xi)| \leq \varepsilon$, the error of the QR can be estimated by

$$|Q_N[g] - Q_N[\tilde{g}]| \leq \sum_{n=0}^N |\omega_n| \cdot |g(\xi_n) - \tilde{g}(\xi_n)| \leq \kappa(\underline{\omega})\varepsilon. \quad (37)$$

Thus, round-off errors due to inexact arithmetics are bounded by the factor $\kappa(\underline{\omega})$. The best possible stability value is given by $\kappa(\underline{\omega}) = I[1]$ for a consistent QR, i.e. $Q_N[1] = I[1]$, and is obtained when all weights are nonnegative. Interpolatory (Newton–Cotes) QRs feature negative weights and their instability intensifies for $N \rightarrow \infty$. Figure 1 illustrates the rising instability of Newton–Cotes QRs as the number of equidistant quadrature points $N + 1$ increases. Here, integration is performed on $[0, 1]$.

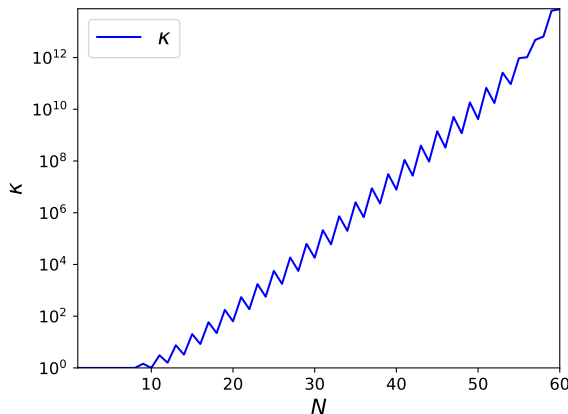


Figure 1: Stability values $\kappa(\underline{\omega})$ for Newton–Cotes QRs

As a result, Newton–Cotes QRs suffer from a major loss of precision when inexact arithmetics are used, due to round-off errors to heavily pollute the computations then. To overcome this problem and construct high-order collocation based DG discretisations on equidistant and scattered points, we propose to use LS-QRs. LS-QRs have been introduced by Wilson in [Wil70b, Wil70a] and — to the best of our knowledge — only have been revisited by Huybrechs in [Huy09]. The idea behind these methods is to allow the number of quadrature points, $N + 1$, to be greater than the order of exactness, d . Then, the resulting linear system of equations that describe the exactness conditions,

$$\underline{A}\underline{\omega} = \underline{m} \quad \text{with} \quad \underline{A} = (\varphi_k(\xi_n))_{k,n=0}^{d,N} \quad \text{and} \quad \underline{m} = (I[\varphi_k])_{k=0}^d, \quad (38)$$

becomes underdetermined. The set of solutions forms a $(N - d)$ -dimensional affine subspace

$$W = \left\{ \underline{\omega} \in \mathbb{R}^{N+1} \mid \underline{A}\underline{\omega} = \underline{m} \right\}, \quad (39)$$

which is generated by $(N - d)$ vectors $\underline{\omega}$ corresponding to distinct interpolatory QRs utilising only $d + 1$ out of the $N + 1$ points. Further note that for every $\underline{\omega} \in W$, the corresponding QR

$$Q_N(g) = \sum_{n=0}^N \omega_n g(\xi_n) \quad (40)$$

provides order of exactness d . We now seek to determine $\underline{\omega}^* \in W$ such that the Euclidean norm

$$\|\underline{\omega}\|_2 := \sqrt{\sum_{n=0}^N |\omega_n|^2} \quad (41)$$

is minimised. Thus, $\underline{\omega}^*$ is given by

$$\underline{\omega}^* = \arg \min_{\underline{\omega} \in W} \|\underline{\omega}\|_2, \quad (42)$$

i. e. as the LS solution of the underdetermined system (38). This solution is obtained by solving

$$\underline{\omega}^* = \underline{\underline{A}}^T \underline{v}, \quad (43)$$

where \underline{v} is the unique solution of the normal equation

$$\underline{\underline{A}}^T \underline{\underline{A}} \underline{v} = \underline{m}. \quad (44)$$

See for instance the book [GVL12] of Golub and Van Loan. Note that when we choose a basis of DOPs w. r. t. the discrete inner product

$$\langle f, g \rangle = \sum_{n=0}^N f(\xi_n) g(\xi_n) \quad (45)$$

in (38), we get $\underline{\underline{A}}^T \underline{\underline{A}} = \underline{\underline{I}}$ and (43) reduces to

$$\underline{\omega}^* = \underline{\underline{A}}^T \underline{m}. \quad (46)$$

Hence, the weights are explicitly given by

$$\omega_n^* = \sum_{k=0}^d \varphi_k(\xi_n) I[\varphi_k] \quad (47)$$

for $n = 0, \dots, N$. It was proven in [Wil70b] that the weights ω_n^* will be nonnegative if a sufficiently large number of quadrature points is used. Thus, the above procedure results in a stable³ QR

$$Q_N[g] = \sum_{n=0}^N \omega_n^* g(\xi_n) \quad (48)$$

with order of exactness d on any set of collocation points. To such QRs (48), we refer to as *LS-QRs*. In the later proposed discretisation of the DG method, we will typically choose $d = 2K$.

³In fact, the QR will even have the optimal stability value of $\kappa = I[1]$.

4. Proposed discretisation of the discontinuous Galerkin method on equidistant and scattered points

In this section, we propose a stable discretisation for (high-order) DG methods on equidistant and scattered points. Therefor, we utilise the techniques discussed in §3, involving DLS approximations, LS-QRs, and bases of DOPs. Starting point of our discretisation is the analytical DG method (14). Transformed to the reference element $\Omega_{\text{ref}} = (-1, 1)$, the task is to find $u^i \in \mathbb{P}_K$ such that

$$\frac{\Delta x_i}{2} \int_{-1}^1 \dot{u}^i v \, d\xi - \int_{-1}^1 f(u^i) v' \, d\xi + f_R^{\text{num}} v(1) - f_L^{\text{num}} v(-1) = 0 \quad (49)$$

for all $v \in \mathbb{P}_k$. Here, u^i denotes the transformation of the numerical solution u , consisting of piecewise polynomials, on the element Ω_i to the reference element. Further, \dot{u}^i denotes the temporal derivative $\partial_t u^i$ and v' the spatial derivative $\partial_x v$. We start our discretisation by replacing $f(u^i)$ in (49) with a polynomial $f^i \in \mathbb{P}_K$ given by a DLS approximation

$$f(u^i) \approx f^i := \sum_{k=0}^K \hat{f}_{k,N}^i \varphi_k, \quad (50)$$

where $\{\varphi_k\}_{k=0}^K$ is a basis of \mathbb{P}_K and the modal coefficients are given by a simple finite sum

$$\hat{f}_{k,N}^i = \left\langle f(u^i), \varphi_k \right\rangle_{\underline{\omega}} = \sum_{n=0}^N \omega_n f(u^i(\xi_n)) \varphi_k(\xi_n). \quad (51)$$

For $N = K$, this is the usual polynomial interpolation. Yet, in our discretisation, N might be chosen greater than K . Next, the involved integrals are replaced by LS-QRs

$$Q_N[g] = \sum_{n=0}^N \omega_n^* g(\xi_n) \approx \int_{-1}^1 g(\xi) \, d\xi \quad (52)$$

as discussed in §3.3. Utilising the discrete inner product $\langle \cdot, \cdot \rangle_{\underline{\omega}^*}$, this results in the discretisation

$$\frac{\Delta x_i}{2} \left\langle \dot{u}^i, v \right\rangle_{\underline{\omega}^*} = \left\langle f^i, v' \right\rangle_{\underline{\omega}^*} - [f_R^{\text{num}} v(1) - f_L^{\text{num}} v(-1)]. \quad (53)$$

$N \in \mathbb{N}$ and $\underline{\omega}^* \in \mathbb{R}^{N+1}$ are chosen such that the resulting LS-QR is stable with $\kappa(\underline{\omega}^*) = 1$ and provides order of exactness $2K$. This will be crucial to prove conservation and linear stability of the resulting discretisation. Further, we follow the idea of collocation and match the quadrature points with the points at which the nodal values of $f(u^i)$ are used to construct the DLS approximation $f^i \in \mathbb{P}_K$. This results in a more efficient implementation of the proposed discretisation. For sake of simplicity, we also use the same weights $\underline{\omega}^*$ for the LS-QR (52) and the DLS approximation (50). Different choices are possible but will not be investigated here. Finally, we include bases of DOPs. Note that we can avoid computing a mass matrix on the left hand side of (53) by utilising such a basis of DOPs w. r. t. the discrete inner product $\langle \cdot, \cdot \rangle_{\underline{\omega}^*}$. Since, when choosing $v = \varphi_l$, we have

$$\left\langle \dot{u}^i, v \right\rangle_{\underline{\omega}^*} = \sum_{k=0}^K \frac{d}{dt} \hat{u}_k^i \langle \varphi_k, \varphi_l \rangle_{\underline{\omega}^*} = \frac{d}{dt} \hat{u}_l^i \quad (54)$$

and (53) becomes a system of $K + 1$ ODEs

$$\frac{\Delta x_i}{2} \frac{d}{dt} \hat{u}_l^i = \left\langle f^i, \varphi_l' \right\rangle_{\underline{\omega}^*} - [f_R^{\text{num}} \varphi_l(1) - f_L^{\text{num}} \varphi_l(-1)] \quad (55)$$

for $l = 0, \dots, K$. The discrete inner product on the right hand side of (55) is given by

$$\langle f^i, \varphi_l' \rangle_{\underline{\omega}^*} = \sum_{k=0}^K \hat{f}_{k,N}^i \langle \varphi_k, \varphi_l' \rangle_{\underline{\omega}^*}. \quad (56)$$

For the sake of brevity, we will refer to the DLS based discretisation (55) of the DG method as the *discontinuous Galerkin discrete least squares (DGDLS) method*. A main part of the DGDLS method is to initially determine a suitable vector of weights $\underline{\omega}^*$ and a corresponding basis of DOPs. Figure 2 provides a flowchart which summarises this procedure.

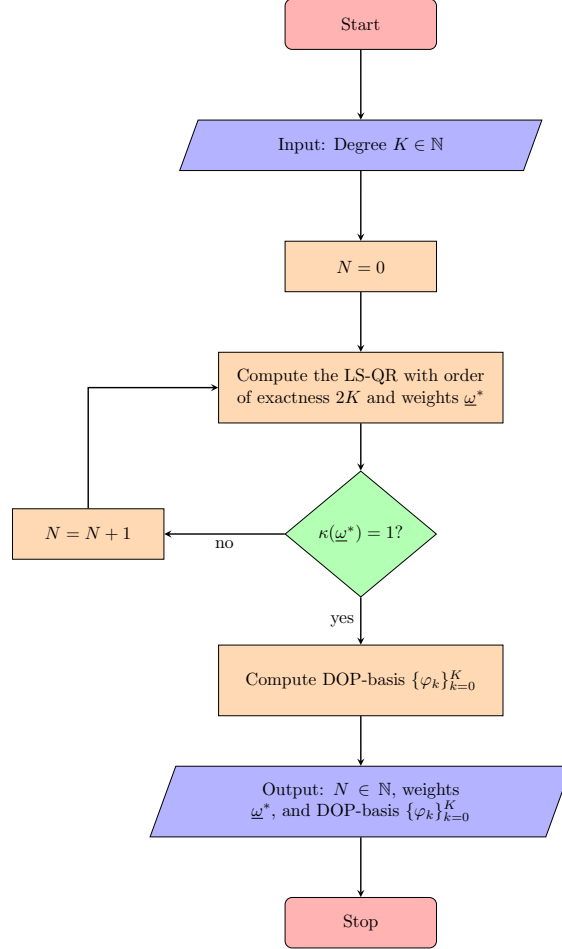


Figure 2: Flowchart describing the initial construction of suitable weights $\underline{\omega}^*$ and a DOP-basis $\{\varphi_k\}_{k=0}^K$

Remark 1. Computing the derivative $\frac{d}{dt} \hat{u}_l^i$ for a fixed $l \in \{0, \dots, K\}$ in the DGDLS method has the following complexity: First note that the inner products $\langle \varphi_k, \varphi_l' \rangle_{\underline{\omega}^*}$ and $\langle \varphi_k, \varphi_l' \rangle_{\underline{\omega}^*}$ respectively in (56) and (51) are computed once-for-all a priori. Thus, the computation of a flux coefficients $\hat{f}_{k,N}^i$ is performed in $\mathcal{O}(N)$ operations and the whole set $\{\hat{f}_{k,N}^i\}_{k=0}^K$, corresponding to a fixed element Ω_i , is computed in $\mathcal{O}(NK)$ operations. This also yields $\frac{d}{dt} \hat{u}_l^i$ in the DGDLS method (55) to be computed in $\mathcal{O}(NK)$ operations. In the subsequent numerical tests, we found the choice $N = 2K$ to be sufficient for a stable computation on equidistant points by the DGDLS method. From point of complexity, this compares to a DG method using over-integration with $2K$ Gauss–Lobatto or Gauss–Legendre points and is by a factor 2 less efficient than a collocation-type DGSEM method using $K + 1$ Gauss–Lobatto or Gauss–Legendre points.

Remark 2. In many methods it is desirable to avoid mass matrices and, in particular, their inversion, see [Abg17, ABT16]. In the proposed discretisation of the DG method this was possible by using bases of DOPs. Continuous Galerkin methods might benefit even more from the combination of DLS approximations and QRs with bases of DOPs. Of course, the restriction to a continuous approximation space has to be regarded. Nevertheless, we believe that the application of DOPs could have a positive impact on these schemes. Future work will investigate this possibility.

5. Conservation and L^2 -stability

In this section, we prove conservation and linear L^2 -stability of the discretisation proposed in §4. Finally, we also give an outlook how entropy stability can be guaranteed.

5.1. Conservation

Let $u \in V_h$ be a numerical solution consisting of a piecewise polynomial of degree at most K of the scalar conservation law

$$u_t + f(u)_x = 0 \quad (57)$$

on $\Omega = [a, b]$. Note that the total amount of the conserved variable u only changes due to the flux across the element boundaries, i. e.

$$\frac{d}{dt} \int_{\Omega} u \, dx = - \left[f(u(b)) - f(u(a)) \right] \quad (58)$$

holds for solutions of (57). We now show that the numerical solution $u \in V_h$ produced by our discretisation (53) of the DG methods also fulfils this property of *conservation*.

The contribution due to a single element Ω_i , transformed to the reference element, is given by

$$\frac{d}{dt} \int_{\Omega_i} u \, dx = \frac{\Delta x_i}{2} \int_{-1}^1 \dot{u}^i \, d\xi, \quad (59)$$

where $u^i = u^i(t, \xi)$ is the transformation of the numerical solution $u = u(t, x)$ on $\Omega_i = (x_{i-1/2}, x_{i+1/2})$ transformed to $\Omega_{\text{ref}} = (-1, 1)$. Further, note that by choosing $v = 1$ in our discretisation (53), we have

$$\frac{\Delta x_i}{2} \langle \dot{u}^i, 1 \rangle_{\underline{\omega}^*} = - \left[f_{i+1/2}^{\text{num}} - f_{i-1/2}^{\text{num}} \right] \quad (60)$$

and since the weights $\underline{\omega}^*$ are related to a QR on the collocation points $\{\xi_n\}_{n=0}^N$ with order of exactness $2K$,

$$\langle \dot{u}^i, 1 \rangle_{\underline{\omega}^*} = Q_N[\dot{u}^i] = \int_{-1}^1 \dot{u}^i \, d\xi \quad (61)$$

holds. Thus, we get

$$\frac{d}{dt} \int_{\Omega_i} u \, dx = \frac{\Delta x_i}{2} \int_{-1}^1 \dot{u}^i \, d\xi = \frac{\Delta x_i}{2} \langle \dot{u}^i, 1 \rangle_{\underline{\omega}^*} = - \left[f_{i+1/2}^{\text{num}} - f_{i-1/2}^{\text{num}} \right]. \quad (62)$$

Finally, summing up over all elements, the rate of change of the total amount of the numerical solution $u \in V_h$ is given by

$$\frac{d}{dt} \int_{\Omega} u \, dx = - \left[f_b^{\text{num}} - f_a^{\text{num}} \right], \quad (63)$$

where $f_b^{\text{num}} = f_{I+1/2}^{\text{num}}$ is the numerical flux at the right boundary of Ω and $f_a^{\text{num}} = f_{1/2}^{\text{num}}$ is the numerical flux at the left boundary of Ω . For a consistent single valued numerical flux, (63) is consistent with (58). Note that for periodic boundary conditions, in particular, we have

$$\frac{d}{dt} \int_{\Omega} u \, dx = 0. \quad (64)$$

This means that for an isolated system, the numerical method is able to exactly mimic the conservation of mass.

5.2. L^2 -stability

Another fundamental design principle for numerical methods is stability. It is well-known that the squared L^2 -norm of physically reasonable solutions of (57) with periodic boundary conditions does not increase over time, i. e.

$$\frac{d}{dt} \|u\|_{L^2}^2 \leq 0, \quad (65)$$

where a strict inequality reflects the presence of shock waves. For scalar conservation laws in one dimension, the squared L^2 -norm is also referred to as the *energy* or the *square entropy*. We now prove that for the linear advection equation

$$u_t + u_x = 0 \quad \text{on} \quad \Omega = [a, b] \quad (66)$$

(strong) L^2 -stability (65) is also fulfilled by our discretisation (53) of the DG method. Therefor, let us assume periodic boundary conditions and let $u \in V_h$ be the numerical solution consisting of a piecewise polynomial of degree at most K . We start by noting that the rate of change of the squared L^2 -norm can be expressed as

$$\frac{d}{dt} \|u\|_{L^2}^2 = 2 \int_{\Omega} u_t u \, dx. \quad (67)$$

In a single element, transformed to the reference element, we have

$$\int_{\Omega_i} u_t u \, dx = \frac{\Delta x_i}{2} \int_{-1}^1 \dot{u}^i u^i \, d\xi. \quad (68)$$

This time choosing $v = u^i$ in (53), results in

$$2 \int_{\Omega_i} u_t u \, dx = \Delta x_i \langle \dot{u}^i, u^i \rangle_{\underline{\omega}^*} = 2 \langle u^i, (u^i)' \rangle_{\underline{\omega}^*} - 2 \left[f_{i+1/2}^{\text{num}} u^i(1) - f_{i-1/2}^{\text{num}} u^i(-1) \right], \quad (69)$$

since $\underline{\omega}^*$ provides a QR with order of exactness $2K$. Further, we have

$$2 \langle u^i, (u^i)' \rangle_{\underline{\omega}^*} = 2 \int_{-1}^1 u^i (u^i)'_{\xi} \, d\xi = (u^i)^2(1) - (u^i)^2(-1) \quad (70)$$

and thus

$$2 \int_{\Omega_i} u_t u \, dx = u^i(1) \left[u^i(1) - 2f_{i+1/2}^{\text{num}} \right] - u^i(-1) \left[u^i(-1) - 2f_{i-1/2}^{\text{num}} \right]. \quad (71)$$

Finally, summing up over all elements, the global rate of change cuts down to a sum of local contributions

$$u_- [u_- - 2f^{\text{num}}] - u_+ [u_+ - 2f^{\text{num}}], \quad (72)$$

where the interface between two neighbouring elements is considered. Here, u_- denotes the value $u^i(1)$ from the left element, u_+ denotes the value $u^{i+1}(-1)$ from the right element, and $f^{\text{num}} = f^{\text{num}}(u_-, u_+)$ denotes the single valued numerical flux at the interface. Using a usual full upwind numerical flux, i.e.

$$f^{\text{num}}(u_-, u_+) = u_-, \quad (73)$$

we get

$$u_- [u_- - 2f^{\text{num}}] - u_+ [u_+ - 2f^{\text{num}}] = -(u_- - u_+)^2 \leq 0. \quad (74)$$

Hence, the proposed discretisation (53) of the DG method is L^2 -stable for the linear advection equation.

5.3. An outlook on entropy stability

Besides L^2 -stability, often methods are desired that also satisfy the more general property of entropy stability. For the DGSEM on Gauss–Lobatto points (including the boundary nodes) a skew-symmetric formulation and SBP operators have been used to prove entropy stability [Gas13, GWK16b, GWK16a]. Recently, Chan, Fernandez, and Carpenter [CDRFC19] proved entropy stability also for a collocation based DG method on Gauss–Legendre nodes (not including the boundary nodes) using a decoupled SBP formulation. They were further able to extend their approach to general selections of quadrature points and various bases. Thus, once we can ensure the SBP property for the proposed DLS discretisation, we could follow the results of Chan, Fernandez, and Carpenter to ensure entropy stability also for the proposed DLS based discretisation of the DG method.

Another option to address entropy stability could be the introduction of entropy correction terms as proposed in [Abg18]. For degree of freedom $k \in \{0, \dots, K\}$ and element $i \in I$, the correction term is given by

$$r_k^i = \alpha(\hat{u}_k^i - \bar{u}^i), \quad (75)$$

where

$$\bar{u} := \frac{1}{K+1} \sum_{k=0}^K \hat{u}_k^i \quad \text{and} \quad \alpha := \frac{E}{\sum_{k=0}^K (\hat{u}_k^i - \bar{u}^i)^2}.$$

Here, E is the so-called entropy error, which can be calculated using an entropy numerical flux \hat{g}^{num} and an entropy variable v^i , which is set equal to the solution u^i for sake of simplicity. Yet, the correction term (75) is also valid for general entropy variables v^i , see [Abg18]. Using (55), E is given by

$$E := [\hat{g}_R^{\text{num}}(1) - \hat{g}_L^{\text{num}}(-1)] - \frac{2}{\Delta x_i} \sum_{k=0}^K \hat{u}_k^i \left(\langle f^i, (u^i)' \rangle_{\omega^*} - [f_R^{\text{num}} u^i(1) - f_L^{\text{num}} u^i(-1)] \right). \quad (76)$$

The correction term is consistent with zero and does not effect the conservation relation since

$$\sum_{k=0}^K r_k^i = \alpha \left(\sum_{k=0}^K (\hat{u}_k^i - \bar{u}) \right) = 0 \quad (77)$$

holds. The correction term (75) is added to the right hand side of the DGDLS scheme (55) and results in an entropy stable scheme. This idea was already applied in [AMO18] to construct entropy stable flux reconstruction schemes on polygonal meshes. Future works will address both approaches to construct entropy stable (DLS based) discretisations of DG methods as well as their comparison.

6. Numerical results

In the subsequent numerical tests, we investigate conservation, L^2 -stability, and approximation properties of the DGDLS methods on equidistant and scattered points. We will do so for a linear advection equation in §6.1 and a nonlinear inviscid Burgers' equation in §6.2. Finally, §6.3 demonstrates the extension to systems of conservation laws and §6.4 addresses a variable coefficients problem in two space dimensions.

6.1. Linear advection equation

Let us consider the linear advection equation

$$u_t + u_x = 0 \quad (78)$$

on $\Omega = [0, 1]$ with a smooth initial condition $u_0(x) = \sin(4\pi x)$ and periodic boundary conditions. By the method of characteristics, the (entropy) solution is simply given by $u(t, x) = u_0(x - t)$. In the following we evolve this solution until time $t = 1$, so that the solution $u(1, x)$ is equal to the initial condition $u_0(x)$.

6.1.1. Conservation and L^2 -stability

We start with a numerical demonstration of conservation and L^2 -stability of the DGDLS method on equidistant and scattered points. Figure 3 illustrates the behaviour of the solution, including its mass and energy over time when equidistant collocation points are used. For this test, we have chosen $I = 5$ equidistant elements, a polynomial degree $K = 3$, and the full upwind numerical flux (73).

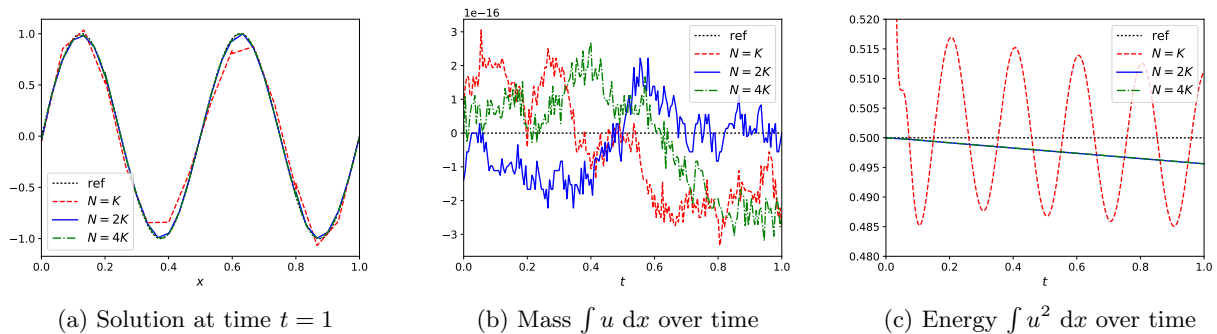


Figure 3: Numerical solution, mass, and energy for $I = 5$, $K = 3$ and $N = K, 2K, 4K$. Linear advection equation and equidistant points.

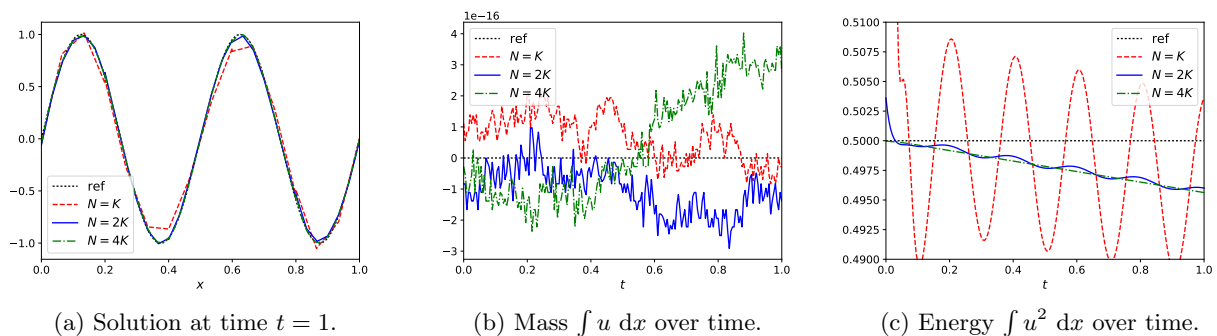


Figure 4: Numerical solution, mass, and energy for $I = 5$, $K = 3$, and $N = K, 2K, 4K$. Linear advection equation and scattered points.

Besides the reference solution, the figures show the numerical solutions for $N = K, 2K, 4K$, i.e. for an increasing number of equidistant points used in the DLS approximation and the LS-QR. All choices yield a conservative method, which can be observed in Figure 3b. Yet, in Figure 3c, we observe the discretisation to be (strongly) L^2 -stable only for $N \geq 2K$. Due to an insufficiently high order of exactness of the LS-QR, the numerical solution for $N = K$ yields spurious oscillation in the energy of the solution over time. As a consequence, the discretisation for $N = 2K$ and $N = 4K$ can be observed to provide more accurate numerical solutions in Figure 3a. We only observe slight differences between the numerical solutions for $N = 2K$ and $N = 4K$. Figure 4 provides a similar demonstration for a set of scattered collocation points. Here, the scattered collocation points are obtained by adding white uniform noise to the set of equidistant collocation points. Thus, the scattered collocation points are given by

$$\tilde{\xi}_0 = -1, \quad \tilde{\xi}_N = 1, \quad \tilde{\xi}_n = \xi_n + Z_n \quad \text{with} \quad \xi_n = -1 + \frac{2n}{N} \quad \text{and} \quad Z_n \in \mathcal{U}\left(-\frac{1}{40N}, \frac{1}{40N}\right), \quad (79)$$

for $n = 1, \dots, N - 1$, where the Z_n are independent, identically distributed, and further assumed to not be correlated with the ξ_n . Using $N = K, 2K, 4K$ scattered collocation points, again, all DLS discretisations

yield a conservative method, see Figure 4b. This time however, slight oscillations can be observed in the energy profile displayed in Figure 4c even for $N = 2K$ collocation points. These oscillations only vanish when going over to a greater set of $N = 4K$ scattered collocation points. This behaviour is again caused by an insufficiently high order of exactness of the QR when scattered points are used. Yet, $N = 2K$ and $N = 4K$ provide similar accurate numerical solutions, as can be observed in Figure 4a.

6.1.2. Accuracy and convergence

Next, we investigate the approximation properties of the proposed discretisation by an error analysis. We consider the same problem as before. Table 1 lists the L^2 -errors for the DGDLS method on equidistant collocation points and an increasing number of degrees of freedom. Table 2 provides the same analysis for sets of scattered collocation points, which are again constructed by adding white uniform noise; see (79). The experimental orders of convergence (EOCs) have been computed by performing a least squares fit for the parameters C and s in the model $y = C \cdot N^{-s}$, where y denotes the L^2 -error for a fixed N .

L^2 -errors						L^2 -errors					
		DGSEM		DGDLS				DGSEM		DGDLS	
K	I	(GL points)	$N = K$	$N = 2K$	$N = 4K$	K	I	(GL points)	$N = 4K$	$N = 16K$	$N = 64K$
1	5	5.8E-1	5.8E-1	6.4E-1	6.4E-1	1	5	5.8E-1	6.4E-1	6.4E-1	6.4E-1
	10	1.0E-1	1.0E-1	2.0E-1	1.9E-1	10	1.0E-1	1.9E-1	1.9E-1	1.9E-1	1.9E-1
	20	2.6E-2	2.6E-2	3.5E-2	3.3E-2	20	2.6E-2	3.3E-2	3.3E-2	3.3E-2	3.3E-2
	40	9.6E-3	9.6E-3	6.4E-3	5.9E-3	40	9.6E-3	5.8E-3	5.7E-3	5.6E-3	5.6E-3
	EOC:	2.5	2.5	1.7	1.8	EOC:	2.4	1.8	1.8	1.8	1.8
2	5	6.6E-2	6.6E-2	1.0E-1	9.9E-2	2	5	6.6E-2	9.9E-2	9.8E-2	9.8E-2
	10	1.0E-2	1.0E-2	8.7E-3	7.9E-3	10	1.0E-2	7.9E-3	7.7E-3	7.6E-3	7.6E-3
	20	1.3E-3	1.3E-3	1.0E-3	9.0E-4	20	1.3E-3	9.0E-4	8.7E-4	8.6E-4	8.6E-4
	40	1.6E-4	1.6E-4	1.2E-4	1.1E-4	40	1.6E-4	1.1E-4	1.0E-4	1.0E-4	1.0E-4
	EOC:	2.7	2.7	3.5	3.6	EOC:	2.7	3.6	3.6	3.6	3.6
3	5	1.1E-2	8.1E-2	1.0E-2	8.9E-3	3	5	1.1E-2	8.9E-3	8.7E-3	8.7E-3
	10	7.6E-4	2.0E-2	6.3E-4	5.4E-4	10	7.6E-4	5.6E-4	5.2E-4	5.2E-4	5.2E-4
	20	4.9E-5	3.8E-4	4.0E-5	3.4E-5	20	4.9E-5	3.7E-5	3.3E-5	3.3E-5	3.3E-5
	40	2.9E-6	3.7E-6	2.5E-6	2.1E-6	40	2.9E-6	2.1E-6	2.0E-6	2.0E-6	2.0E-6
	EOC:	3.8	2.1	3.9	4.0	EOC:	3.8	3.9	4.0	4.0	4.0
4	5	1.3E-3	1.1E-2	1.2E-3	1.0E-3	4	5	1.3E-3	1.1E-3	1.0E-3	1.0E-3
	10	5.1E-5	4.3E-3	4.2E-5	3.4E-5	10	5.1E-5	3.8E-4	4.3E-5	3.3E-5	3.3E-5
	20	2.3E-6	9.0E-4	1.5E-6	1.2E-6	20	2.3E-6	3.9E-4	5.8E-6	2.0E-6	2.0E-6
	40	1.1E-7	9.1E-5	1.0E-7	9.7E-8	40	1.1E-7	4.6E-6	6.4E-6	2.7E-7	2.7E-7
	EOC:	4.1	1.5	4.1	4.1	EOC:	4.1	1.1	4.0	4.1	4.1

Table 1: Linear advection equation & equidistant points.

Table 2: Linear advection equation & scattered points.

We note from both tables that increasing the number of collocation points does not always yield more accurate numerical solutions when using a fairly small number of degrees of freedom, i. e. polynomials of degree $K = 1$ or only $I = 5$ elements. Yet, for all higher degrees $K \geq 2$ (and $I > 5$ for $K = 2$), we observe the numerical solutions to become more accurate when the number of collocation points is increased. Further, both tables provide a comparison of the DGDLS method with the usual DGSEM on a set of Gauss–Lobatto points. The DGSEM can be considered as a special case of the proposed DGDLS method when Gauss–Lobatto points are used and $N = K$ is chosen, i. e. using polynomial interpolation as well as an interpolatory (Gauss–Lobatto) QR. Of course, Gauss–Lobatto points and their corresponding QR are known to be superior to equidistant or even scattered points, at least when the same number of points is used. Yet, when sufficiently increasing the number of collocation points, we often observe the DGDLS method to provide more accurate results on equidistant and even scattered collocation points than the DGSEM on Gauss–Lobatto points.

Remark 3. In some cases, we observe the error to increase even though the number of elements I is increased, e. g. for $K = 4$ and $N = 4K$ when going over from $I = 10$ to $I = 20$ as well as for $K = 4$ and

$N = 16K$ when going over from $I = 20$ to $I = 40$ in Table 2. The same observation can be made for the subsequent tables 3 and 4 concerning the inviscid Burgers' equation. This behaviour is caused by the instability of the LS-QR when an insufficiently great number of collocation points N is used. Hence, we observe this problem to vanish when N is increased; see the case $N = 64$ in tables 2 and 4.

6.2. Inviscid Burgers' equation

Let us now consider the nonlinear inviscid Burgers' equation

$$u_t + \left(\frac{u^2}{2} \right)_x = 0 \quad (80)$$

on $\Omega = [0, 1]$ with smooth initial condition $u_0(x) = 1 + \frac{1}{4\pi} \sin(2\pi x)$ and periodic boundary conditions. For this problem a shock develops in the solution when the wave breaks at time

$$t_b = -\frac{1}{\min_{0 \leq x \leq 1} u'_0(x)} = 2. \quad (81)$$

In the subsequent numerical tests we consider the solution at times $t = 1$ and $t = 3$. This time, a local Lax–Friedrichs (LLF) numerical flux

$$f_{LLF}^{\text{num}}(u_-, u_+) = \frac{1}{2} [f(u_-) + f(u_+)] - \frac{\lambda}{2} \cdot (u_+ - u_-) \quad \text{with} \quad \lambda = \max\{|u_-|, |u_+|\} \quad (82)$$

is used at the element interfaces. The reference solutions have been computed using characteristic tracing, solving the implicit equation $u(t, x) = u_0(x - tu)$ in smooth regions. The jump location, separating these regions, can be determined by the Rankine–Hugoniot condition.

6.2.1. Conservation and L^2 -stability

Again, we start with a numerical investigation of conservation and L^2 -stability. Note that our proof of L^2 -stability in §5.2 only addresses the linear advection equation. Still, we observe similar results for the nonlinear Burgers' equations. These results are illustrated in Figure 5 for a set of equidistant collocation points and in Figure 6 for a set of scattered collocation points, constructed by adding white uniform noise as described in (79).

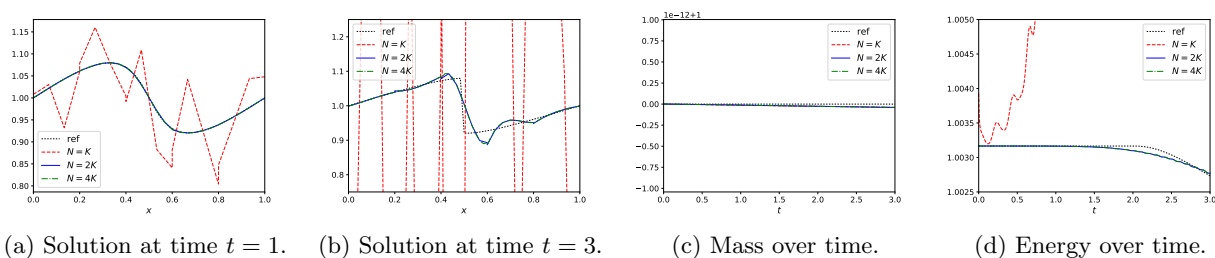


Figure 5: Numerical solution, mass, and energy for $I = 5$, $K = 3$, and $N = K, 2K, 4K$. Burgers' equation and equidistant points.

Figures 5a and 6a show the solutions of the DGDLS method at time $t = 1$. At this time, no discontinuity has developed and the solution is still smooth. For the case of equidistant collocation points in Figure 5a, the DGDLS method for $N = 2K, 4K$ is observed to provide reasonable numerical solutions. However, the numerical solution for $N = K$ shows heavy oscillations. The same can be observed for numerical solutions for $N = K$ as well as $N = 2K$ when scattered collocation points are used in Figure 6a. Here, only the numerical solution for $N = 4K$ can be considered as reasonable. A similar observation can be made for both kinds of collocation points at time $t = 3$. In the case of scattered collocation points,

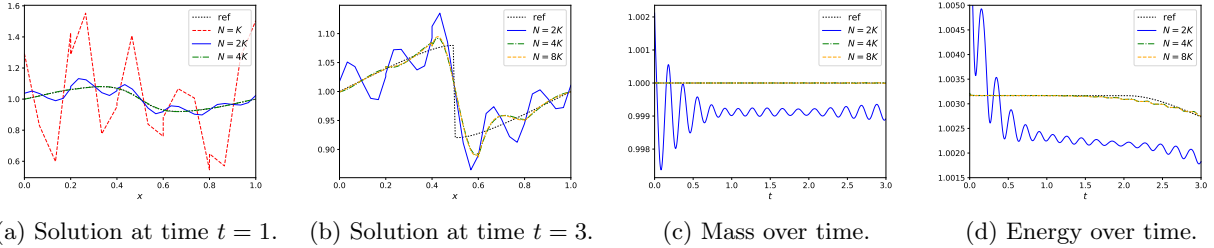


Figure 6: Numerical solution, mass, and energy for $I = 5$, $K = 3$, and $N = K, 2K, 4K$. Burgers' equation and scattered points.

the computation even broke down for $N = K$. Thus, Figure 6b instead illustrates the results for $N = 2K, 4K, 8K$. Note that all numerical results for $t = 3$, also the ones for equidistant collocation points in Figure 5b, show at least some minor oscillations. This is a common problem for high-order methods and might be overcome by post-processing (assuming a stable computation until the final time has been reached) or additional shock-capturing. Shock-capturing might be performed, for instance, by artificial viscosity methods [PP06, KWH11, GNA⁺19, RGÖS18], modal filtering [Van91, HK08, MOSW13, GÖS18], finite volume subcells [HCP12, SM14, DZLD14, MO16], or other methods [GG19, Gla19]. Shock capturing in DLS based high-order methods might be investigated in future works. Finally, when a sufficiently great number of collocation points is used, we again observe the mass of the numerical solutions to nearly remain constant, see Figures 5c and 6c, and the energy to nearly remain constant until the discontinuity occurs at time $t = 2$ and to decrease afterwards, see Figures 5d and 6d.

6.2.2. Accuracy and convergence

We continue the above investigation of the DGDLS method by providing an additional error analysis. Tables 3 and 4 respectively list the errors for DGDLS method at time $t = 1$ on equidistant and scattered points. We note that the DGDLS method for $N = K$ does not yield stable numerical solutions. Yet, we again observe that increasing the number of collocation points in the DGDLS method results in more accurate numerical solutions. At least for equidistant collocation points, the DGDLS method even yields more accurate numerical solutions than the DGSEM on Gauss-Lobatto points.

Further, in both cases, we are able to recover or even exceed the EOC of the DGSEM when a sufficiently great number of collocation points is used.

6.3. Extension to systems: The wave equation

The extension of the DGDLS method to systems of conservation laws is the same as for most discretisations of the DG method, we simply apply the discretisation proposed in §4 to every component of the system separately. As a representative, we consider the second order scalar wave equation in one dimension

$$u_{tt} - c^2 u_{xx} = 0 \quad (83)$$

on $\Omega = [0, 1]$ with periodic boundary conditions. The wave equation (83) can be rewritten as a first-order system of conservation laws

$$\begin{aligned} u_t + cv_x &= 0, \\ v_t + cu_x &= 0, \end{aligned} \quad (84)$$

which is sometimes referred to as the one dimensional acoustic problem [GPR08]. Given initial conditions $u(0, x) = u_0(x)$ and $v(0, x) = v_0(x)$, the solution is given by

$$\begin{aligned} u(t, x) &= \frac{1}{2} [u_0(x - ct) + u_0(x + ct)] + \frac{1}{2} [v_0(x - ct) - v_0(x + ct)], \\ v(t, x) &= \frac{1}{2} [u_0(x - ct) - u_0(x + ct)] + \frac{1}{2} [v_0(x - ct) + v_0(x + ct)]. \end{aligned} \quad (85)$$

L^2 -errors					
DGSEM			DGDLS		
K	I	(GL points)	$N = K$	$N = 2K$	$N = 4K$
1	5	1.3E-2	1.3E-2	1.1E-2	1.2E-2
	10	3.8E-3	3.8E-3	4.1E-3	3.8E-3
	20	1.1E-3	1.1E-3	9.3E-4	8.7E-4
	40	2.8E-4	2.8E-4	2.0E-4	1.8E-4
	EOC:	1.8	1.8	1.5	1.7
2	5	1.7E-3	1.7E-3	3.4E-3	3.0E-3
	10	5.9E-4	5.9E-4	3.4E-4	3.5E-4
	20	6.7E-5	6.7E-5	5.0E-5	4.5E-5
	40	8.0E-6	8.0E-6	6.2E-6	5.5E-6
	EOC:	1.7	1.7	3.3	3.0
3	5	1.0E-3	7.1E-2	4.9E-4	6.7E-4
	10	9.4E-5	4.2E-1	8.3E-5	7.5E-5
	20	5.8E-6	NaN	5.6E-6	4.7E-6
	40	3.6E-7	NaN	3.0E-7	2.6E-7
	EOC:	3.4	-	2.6	3.1
4	5	1.9E-4	NaN	4.3E-4	3.1E-4
	10	1.0E-5	NaN	1.3E-5	1.1E-5
	20	3.7E-7	NaN	2.2E-7	2.2E-7
	40	1.9E-8	NaN	1.8E-8	1.4E-8
	EOC:	4.2	-	4.3	4.4

L^2 -errors					
DGSEM			DGDLS		
K	I	(GL points)	$N = 4K$	$N = 16K$	$N = 64K$
1	5	1.3E-2	1.2E-2	1.2E-2	1.2E-2
	10	1.3E-2	3.9E-3	3.7E-3	3.7E-3
	20	1.1E-3	8.6E-4	8.5E-4	8.4E-4
	40	2.8E-4	1.9E-4	1.8E-4	1.7E-4
	EOC:	0.8	1.7	1.7	1.7
2	5	1.7E-3	3.0E-3	2.9E-3	2.9E-3
	10	5.9E-4	1.3E-3	3.5E-4	3.5E-4
	20	6.7E-5	1.3E-4	4.9E-5	4.4E-5
	40	8.0E-6	3.6E-4	6.9E-5	9.9E-6
	EOC:	1.7	1.3	3.0	3.0
3	5	1.0E-3	9.1E-4	7.1E-4	6.9E-4
	10	9.4E-5	5.0E-4	9.9E-5	7.2E-5
	20	5.8E-6	4.4E-4	1.1E-5	4.9E-6
	40	3.6E-7	3.1E-4	7.7E-6	3.0E-6
	EOC:	3.4	0.5	2.8	3.2
4	5	1.9E-4	7.5E-4	3.5E-4	3.0E-4
	10	1.0E-5	9.1E-4	6.0E-5	1.3E-5
	20	3.7E-7	2.2E-3	1.7E-4	9.2E-6
	40	1.9E-8	1.7E-4	6.6E-5	8.5E-6
	EOC:	4.2	0.0	0.9	4.2

Table 3: Burgers' equation at $t = 1$ & equidistant points.

Table 4: Burgers' equation at $t = 1$ & scattered points.

In the subsequent numerical tests we choose $c = 1$ and consider the initial conditions $u_0(x) = e^{-20(2x-1)^2}$ and $v_0(x) = 0$. For the numerical flux, we have used an upwind flux

$$f^{\text{num}} = \frac{1}{2} \left((v^- + v^+) - (u^+ - u^-) \right). \quad (86)$$

Figures 7 and 8 illustrate the pointwise errors of the DGDLS method for a longtime simulation. We have

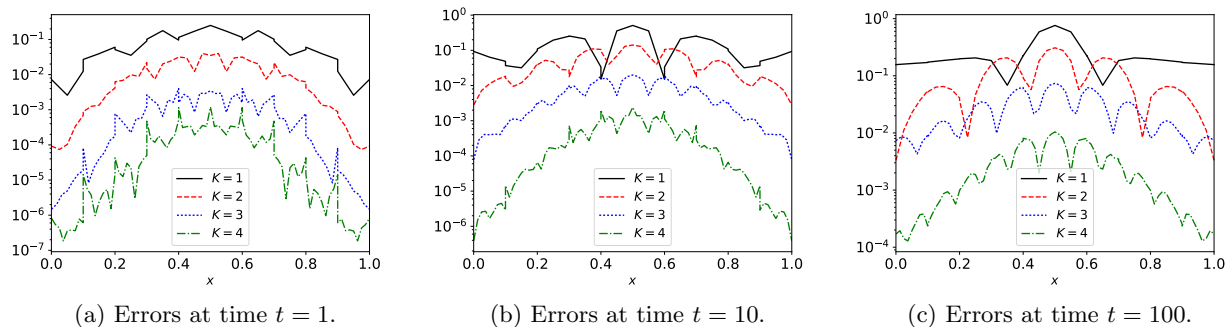


Figure 7: Pointwise errors over time for the wave equation. DGDLS method for $I = 10$, $N = 2K$, $K = 1, 2, 3, 4$, and equidistant collocation points.

used $I = 20$ elements and an increasing polynomial degree $K = 1, 2, 3, 4$ in all computations. Further, for equidistant points in Figure 7 we have used $N = 2K$ collocation points and for the case of scattered points in Figure 8 we have used $N = 4K$ collocation points. The figures show the pointwise errors

$$E(t, x) := |u(t, x) - u_{\text{num}}(t, x)| + |v(t, x) - v_{\text{num}}(t, x)| \quad (87)$$

for times $t = 1, 10, 100$. We note that the DGDLS method, regardless of whether equidistant or scattered collocation points are used, yields accurate results even for longtime simulations, especially when higher

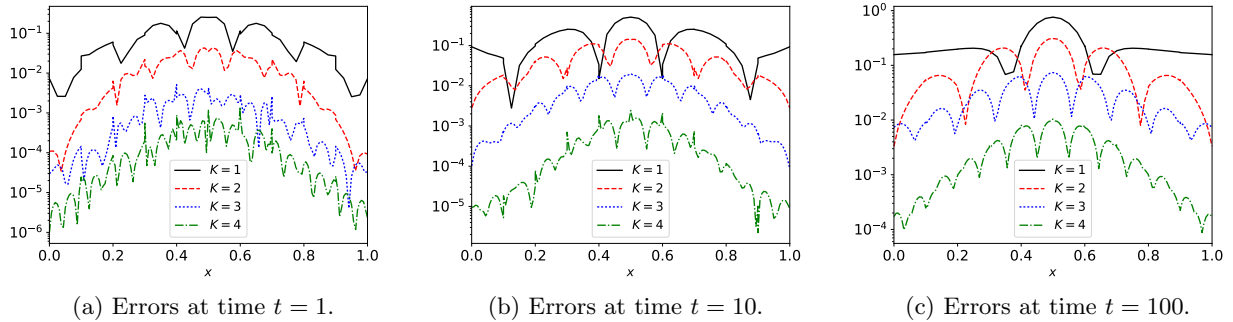


Figure 8: Pointwise errors over time for the wave equation. DGDLS method for $I = 10$, $N = 4K$, $K = 1, 2, 3, 4$, and scattered collocation points.

polynomial degrees are used. Future work might include a more detailed investigation of long-time error behaviour as, for instance, performed in [KNG17, ÖR19].

6.4. Extension to multiple dimensions: Linear advection equation with variable coefficients

In this subsection, we address the extension of the proposed DGDLS method to multiple dimensions by extending the ideas from the one dimensional case using a tensor product grid; see [Tra09, Chapter 7.1.6]. Let us consider the linear advection equation in two dimensions

$$u_t + (au)_x + (bu)_y = 0 \quad (88)$$

with variable coefficients $a = a(x, y)$ and $b = b(x, y)$ on $\Omega = [0, 1]^2 \subset \mathbb{R}^2$. Here, we choose $a(x) = x$ and $b(x) = 1$ together with initial condition

$$u_0(x, y) = \sin(4\pi x) \left(1 - \frac{1}{2} \sin(2\pi y) \right) \quad (89)$$

and boundary conditions

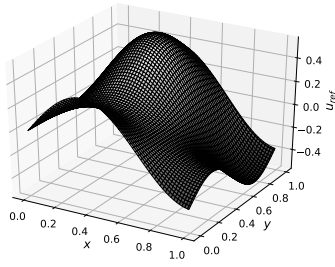
$$u(t, x, 0) = u(t, x, 1), \quad (90)$$

$$u(t, 0, y) = 0. \quad (91)$$

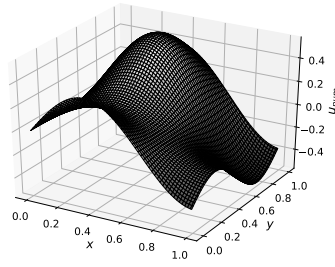
Note that (90) corresponds to periodic boundary conditions at the upper and lower boundary of Ω , while (91) corresponds to a physical inflow boundary condition at the left boundary of Ω . The solution of the corresponding Cauchy problem can be calculated by the method of characteristics (see [Bre00, Chapter 3]) and is given by

$$\begin{aligned} u(t, x, y) &= \exp(-t) u_0(x \exp(-t), y) \\ &= \exp(-t) \sin(4\pi x \exp(-t)) \left(1 - \frac{1}{2} \sin(2\pi y) \right). \end{aligned} \quad (92)$$

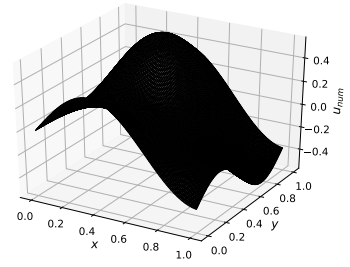
Figure 9 and 10 respectively illustrate different surface and contour plots. Both figures demonstrate that the DGDLS method using $I = 20$ rectangular elements, a polynomial degree of $K = 3$ and $N = 2K$ equidistant collocation points in each direction yields numerical solutions which are in good agreement with the reference solution (92). When using $N = 2K$ scattered collocation points in each direction, the DGDLS method produces numerical solutions with slight oscillations; see Figure 9e for the surface plot and Figure 10e for the corresponding contour plot. Yet, when going over to a greater number of $N = 4K$ scattered collocation points in each direction, the DGDLS method again yields numerical solutions which are in good agreement with the reference solution.



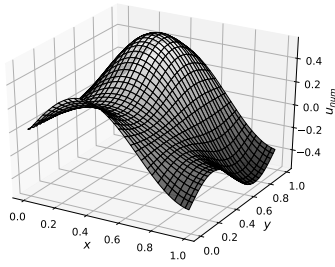
(a) Reference solution.



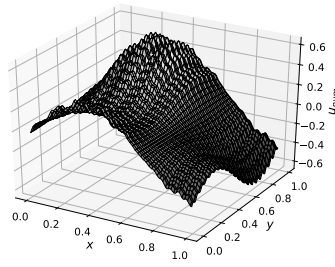
(b) DGDLS, equid. points, $N = 2K$.



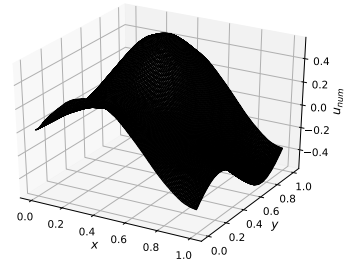
(c) DGDLS, equid. points, $N = 4K$.



(d) DGSEM, Gauss-Lobatto points.

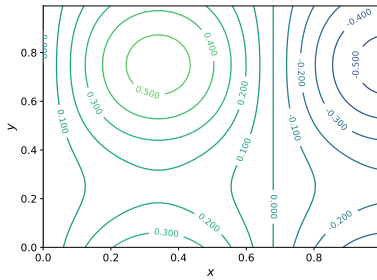


(e) DGDLS, scat. points, $N = 2K$.

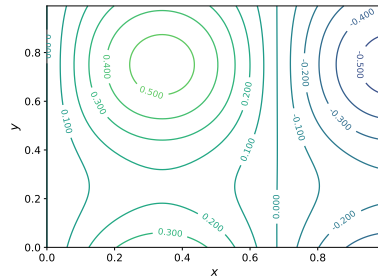


(f) DGDLS, scat. points, $N = 4K$.

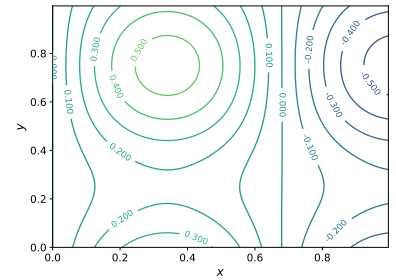
Figure 9: Surface plots of the solution at time $t = 1$. For the DGSEM and DGDLS method, a polynomial degree of $K = 3$ and $I = 20$ rectangular elements have been used in each direction.



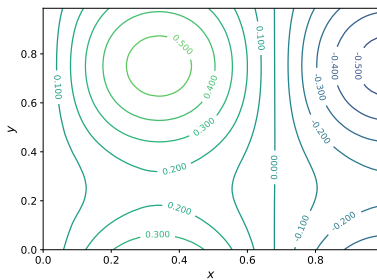
(a) Reference solution.



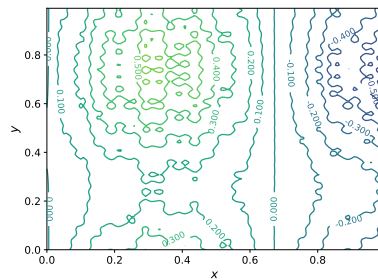
(b) DGDLS, equid. points, $N = 2K$.



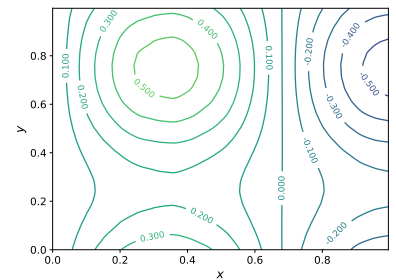
(c) DGDLS, equid. points, $N = 4K$.



(d) DGSEM, Gauss-Lobatto points.



(e) DGDLS, scat. points, $N = 2K$.



(f) DGDLS, scat. points, $N = 4K$.

Figure 10: Contour plots of the solution at time $t = 1$. For the DGSEM and DGDLS method, a polynomial degree of $K = 3$ and $I = 20$ rectangular elements have been used in each direction.

7. Summary

In this work, we have proposed and investigated stable collocation-type discretisations of the DG method on equidistant and scattered collocation points. We have done so by utilising DLS approximations instead of usual polynomial interpolation and LS-QRs, providing stable high-order numerical integration even on equidistant and scattered points. In §5, we have proved conservation and linear L^2 -stability of the proposed DGDLS method. In several numerical tests we have observed that the DGDLS method on equidistant points is able to recover — sometimes even to exceed — the accuracy and EOC of the usual DGSEM on Gauss–Lobatto points. Finally, the extension to the nonlinear viscous Burgers’ equation, systems of conservation laws, and long time simulations, and a variable coefficient problem in two dimensions using a tensor product approach have been demonstrated. Future work will address more general entropy stability and the extension to unstructured meshes, such as triangles and nonconvex polygons.

Acknowledgements

The first author would like to thank the Max Planck Institute for Mathematics (MPIM) Bonn for wonderful working conditions. Further, the first author was supported by the German Research Foundation (DFG, Deutsche Forschungsgemeinschaft) under Grant SO 363/15-1.

The second author was supported by SNF project (Number 175784) “Solving advection dominated problems with high order schemes with polygonal meshes: application to compressible and incompressible flow problems”.

References

- [Abg17] R. Abgrall. High order schemes for hyperbolic problems using globally continuous approximation and avoiding mass matrices. *Journal of Scientific Computing*, 73(2-3):461–494, 2017.
- [Abg18] R. Abgrall. A general framework to construct schemes satisfying additional conservation relations. Application to entropy conservative and entropy dissipative schemes. *Journal of Computational Physics*, 372:640–666, 2018.
- [ABT16] R. Abgrall, P. Bacigaluppi, and S. Tokareva. How to avoid mass matrix for linear hyperbolic problems. In *Numerical Mathematics and Advanced Applications ENUMATH 2015*, pages 75–86. Springer, 2016.
- [AMO18] R. Abgrall, E. I. Meledo, and P. Oeffner. On the connection between residual distribution schemes and flux reconstruction. *arXiv preprint arXiv:1807.01261*, 2018.
- [Bre00] A. Bressan. *Hyperbolic systems of conservation laws: the one-dimensional Cauchy problem*, volume 20. Oxford University Press on Demand, 2000.
- [CDRFC19] J. Chan, D. C. Del Rey Fernández, and M. H. Carpenter. Efficient entropy stable Gauss collocation methods. *SIAM Journal on Scientific Computing*, 41(5):A2938–A2966, 2019.
- [CHS90] B. Cockburn, S. Hou, and C.-W. Shu. The Runge–Kutta local projection discontinuous Galerkin finite element method for conservation laws. IV. The multidimensional case. *Mathematics of Computation*, 54(190):545–581, 1990.
- [CLS89] B. Cockburn, S.-Y. Lin, and C.-W. Shu. TVB Runge–Kutta local projection discontinuous Galerkin finite element method for conservation laws III: one-dimensional systems. *Journal of Computational Physics*, 84(1):90–113, 1989.
- [CS89] B. Cockburn and C.-W. Shu. TVB Runge–Kutta local projection discontinuous Galerkin finite element method for conservation laws. II. General framework. *Mathematics of Computation*, 52(186):411–435, 1989.
- [CS91] B. Cockburn and C.-W. Shu. The Runge–Kutta local projection P^1 -discontinuous-Galerkin finite element method for scalar conservation laws. *ESAIM: Mathematical Modelling and Numerical Analysis*, 25(3):337–361, 1991.
- [CS98] B. Cockburn and C.-W. Shu. The Runge–Kutta discontinuous Galerkin method for conservation laws V: multi-dimensional systems. *Journal of Computational Physics*, 141(2):199–224, 1998.
- [DZLD14] M. Dumbser, O. Zanotti, R. Loubère, and S. Diot. A posteriori subcell limiting of the discontinuous Galerkin finite element method for hyperbolic conservation laws. *Journal of Computational Physics*, 278:47–75, 2014.
- [Gas13] G. J. Gassner. A skew-symmetric discontinuous Galerkin spectral element discretization and its relation to SBP-SAT finite difference methods. *SIAM Journal on Scientific Computing*, 35(3):A1233–A1253, 2013.
- [Gau04] W. Gautschi. *Orthogonal polynomials: Computation and approximation*. Oxford University Press on Demand, 2004.
- [Gau11] W. Gautschi. *Numerical analysis*. Springer Science & Business Media, 2011.
- [GG19] J. Glaubitz and A. Gelb. High order edge sensors with ℓ^1 regularization for enhanced discontinuous Galerkin methods. *SIAM Journal on Scientific Computing*, 41(2):A1304–A1330, 2019.
- [GKS11] S. Gottlieb, D. I. Ketcheson, and C.-W. Shu. *Strong stability preserving Runge–Kutta and multistep time discretizations*. World Scientific, 2011.

- [Gla19] J. Glaubitz. Shock capturing by Bernstein polynomials for scalar conservation laws. *Applied Mathematics and Computation*, 363:124593, 2019.
- [GNA⁺19] J. Glaubitz, A. Nogueira, J. Almeida, R. Cantão, and C. Silva. Smooth and compactly supported viscous sub-cell shock capturing for discontinuous Galerkin methods. *Journal of Scientific Computing*, 79(1):249–272, 2019.
- [GÖS18] J. Glaubitz, P. Öffner, and T. Sonar. Application of modal filtering to a spectral difference method. *Mathematics of Computation*, 87(309):175–207, 2018.
- [GPR08] A. Gelb, R. B. Platte, and W. S. Rosenthal. The discrete orthogonal polynomial least squares method for approximation and solving partial differential equations. *Communications in Computational Physics*, 3(3):734–758, 2008.
- [GS98] S. Gottlieb and C.-W. Shu. Total variation diminishing Runge–Kutta schemes. *Mathematics of Computation of the American Mathematical Society*, 67(221):73–85, 1998.
- [GST01] S. Gottlieb, C.-W. Shu, and E. Tadmor. Strong stability-preserving high-order time discretization methods. *SIAM review*, 43(1):89–112, 2001.
- [GVL12] G. H. Golub and C. F. Van Loan. *Matrix computations*, volume 3. JHU Press, 2012.
- [GWK16a] G. J. Gassner, A. R. Winters, and D. A. Kopriva. Split form nodal discontinuous Galerkin schemes with summation-by-parts property for the compressible Euler equations. *Journal of Computational Physics*, 327:39–66, 2016.
- [GWK16b] G. J. Gassner, A. R. Winters, and D. A. Kopriva. A well balanced and entropy conservative discontinuous Galerkin spectral element method for the shallow water equations. *Applied Mathematics and Computation*, 272:291–308, 2016.
- [HCP12] A. Huerta, E. Casoni, and J. Peraire. A simple shock-capturing technique for high-order discontinuous Galerkin methods. *International Journal for Numerical Methods in Fluids*, 69(10):1614–1632, 2012.
- [HK08] J. Hesthaven and R. Kirby. Filtering in Legendre spectral methods. *Mathematics of Computation*, 77(263):1425–1452, 2008.
- [Huy09] D. Huybrechs. Stable high-order quadrature rules with equidistant points. *Journal of Computational and Applied Mathematics*, 231(2):933–947, 2009.
- [HW07] J. S. Hesthaven and T. Warburton. *Nodal discontinuous Galerkin methods: algorithms, analysis, and applications*. Springer Science & Business Media, 2007.
- [JS94] G. S. Jiang and C.-W. Shu. On a cell entropy inequality for discontinuous Galerkin methods. *Mathematics of Computation*, 62(206):531–538, 1994.
- [Ket08] D. I. Ketcheson. Highly efficient strong stability-preserving Runge–Kutta methods with low-storage implementations. *SIAM Journal on Scientific Computing*, 30(4):2113–2136, 2008.
- [KG14] D. A. Kopriva and G. J. Gassner. An energy stable discontinuous Galerkin spectral element discretization for variable coefficient advection problems. *SIAM Journal on Scientific Computing*, 36(4):A2076–A2099, 2014.
- [KK03] R. M. Kirby and G. E. Karniadakis. De-aliasing on non-uniform grids: algorithms and applications. *Journal of Computational Physics*, 191(1):249–264, 2003.
- [KNG17] D. A. Kopriva, J. Nordström, and G. J. Gassner. Error boundedness of discontinuous Galerkin spectral element approximations of hyperbolic problems. *Journal of Scientific Computing*, 72(1):314–330, 2017.
- [Kop09] D. A. Kopriva. *Implementing spectral methods for partial differential equations: Algorithms for scientists and engineers*. Springer Science & Business Media, 2009.
- [KS74] H.-O. Kreiss and G. Scherer. Finite element and finite difference methods for hyperbolic partial differential equations. In *Mathematical aspects of finite elements in partial differential equations*, pages 195–212. Elsevier, 1974.
- [KS06] V. I. Krylov and A. H. Stroud. *Approximate calculation of integrals*. Courier Corporation, 2006.
- [KWH11] A. Klöckner, T. Warburton, and J. S. Hesthaven. Viscous shock capturing in a time-explicit discontinuous Galerkin method. *Mathematical Modelling of Natural Phenomena*, 6(3):57–83, 2011.
- [LeV02] R. J. LeVeque. *Finite volume methods for hyperbolic problems*, volume 31. Cambridge university press, 2002.
- [LT98] D. Levy and E. Tadmor. From Semidiscrete to Fully Discrete: Stability of Runge–Kutta Schemes by The Energy Method. *SIAM review*, 40(1):40–73, 1998.
- [MO16] A. Meister and S. Ortleb. A positivity preserving and well-balanced DG scheme using finite volume subcells in almost dry regions. *Applied Mathematics and Computation*, 272:259–273, 2016.
- [MOSW13] A. Meister, S. Ortleb, T. Sonar, and M. Wirz. An extended discontinuous Galerkin and spectral difference method with modal filtering. *ZAMM-Journal of Applied Mathematics and Mechanics/Zeitschrift für Angewandte Mathematik und Mechanik*, 93(6-7):459–464, 2013.
- [NC99] J. Nordström and M. H. Carpenter. Boundary and interface conditions for high-order finite-difference methods applied to the Euler and Navier–Stokes equations. *Journal of Computational Physics*, 148(2):621–645, 1999.
- [ÖGR19] P. Öffner, J. Glaubitz, and H. Ranocha. Stability of correction procedure via reconstruction with summation-by-parts operators for Burgers’ equation using a polynomial chaos approach. *ESAIM: Mathematical Modelling and Numerical Analysis (ESAIM: M2AN)*, 52(6):2215–2245, 02 2019.
- [Ols95a] P. Olsson. Summation by parts, projections, and stability. I. *Mathematics of Computation*, 64(211):1035–1065, 1995.
- [Ols95b] P. Olsson. Summation by parts, projections, and stability. II. *Mathematics of Computation*, 64(212):1473–1493, 1995.
- [ÖR19] P. Öffner and H. Ranocha. Error boundedness of discontinuous Galerkin methods with variable coefficients. *Journal of Scientific Computing*, pages 1–36, 2019.

- [PP06] P.-O. Persson and J. Peraire. Sub-cell shock capturing for discontinuous Galerkin methods. In *44th AIAA Aerospace Sciences Meeting and Exhibit*, page 112, 2006.
- [PTK11] R. B. Platte, L. N. Trefethen, and A. B. Kuijlaars. Impossibility of fast stable approximation of analytic functions from equispaced samples. *SIAM review*, 53(2):308–318, 2011.
- [RGÖS18] H. Ranocha, J. Glaubitz, P. Öffner, and T. Sonar. Stability of artificial dissipation and modal filtering for flux reconstruction schemes using summation-by-parts operators. *Applied Numerical Mathematics*, 128:1–23, 2018.
- [RH73] W. H. Reed and T. Hill. Triangular mesh methods for the neutron transport equation. Technical report, Los Alamos Scientific Lab., N. Mex.(USA), 1973.
- [RÖS16] H. Ranocha, P. Öffner, and T. Sonar. Summation-by-parts operators for correction procedure via reconstruction. *Journal of Computational Physics*, 311:299–328, 2016.
- [Run01] C. Runge. Über empirische Funktionen und die Interpolation zwischen äquidistanten Ordinaten. *Zeitschrift für Mathematik und Physik*, 46(224-243):20, 1901.
- [SM14] M. Sonntag and C.-D. Munz. Shock capturing for discontinuous Galerkin methods using finite volume subcells. In *Finite Volumes for Complex Applications VII-Elliptic, Parabolic and Hyperbolic Problems*, pages 945–953. Springer, 2014.
- [Str94] B. Strand. Summation by parts for finite difference approximations for d/dx . *Journal of Computational Physics*, 110(1):47–67, 1994.
- [TBI97] L. N. Trefethen and D. Bau III. *Numerical linear algebra*, volume 50. Siam, 1997.
- [Tor13] E. F. Toro. *Riemann solvers and numerical methods for fluid dynamics: a practical introduction*. Springer Science & Business Media, 2013.
- [Tra09] J. A. Trangenstein. *Numerical solution of hyperbolic partial differential equations*. Cambridge University Press, 2009.
- [Van91] H. Vandeven. Family of spectral filters for discontinuous problems. *Journal of Scientific Computing*, 6(2):159–192, 1991.
- [Wil70a] M. W. Wilson. Discrete least squares and quadrature formulas. *Mathematics of Computation*, 24(110):271–282, 1970.
- [Wil70b] M. W. Wilson. Necessary and sufficient conditions for equidistant quadrature formula. *SIAM Journal on Numerical Analysis*, 7(1):134–141, 1970.